Partial decomposition of TiH_2 studied in situ by energy dispersive diffraction and ex situ by diffraction microtomography of hard X-ray synchrotron radiation

C. Jiménez[1,2], F. Garcia-Moreno[1,2], A. Rack[3], R. Tucoulou[3], M. Klaus[2], B. Pfretzschner[1,2], T. Rack[4], P. Cloetens[3], J. Banhart[1,2]

[1] Technische Universität Berlin, Hardenbergstr. 36, 10623 Berlin, Germany

[2] Helmholtz-Zentrum Berlin für Materialien und Energie, Hahn-Meitner-Platz 1, 14109 Berlin, Germany

[3] European Synchrotron Radiation Facility, BP 220, 38043 Grenoble, France

[4] Charité Berlin, Charitéplatz 1, 10117 Berlin, Germany

ABSTRACT

Phase transformations of TiH_2 powder during its partial decomposition were followed by in situ diffraction and compared to thermoanalytical traces. During *heating* endothermic peaks of H_2 release are correlated with mass loss regimes and phase transformation sequence, in which the phases α+δ+β co-exist. During *cooling* the exothermic transformation $\alpha+\beta \xrightarrow{232\pm7\,^{\circ}C} \alpha+\delta$ occurs without mass loss, which suppresses the co-existence of α+δ+β. Microtomography revealed a resulting heterogeneous distribution of δ lamellae embedded by an α matrix inside the particles in proportions 30:70 (vol.%).

TiH_2 powder can be used for foaming low melting Al- [1, 2], Zn- [3, 4] or Mg-based [5] alloys. As-received TiH_2 powder is commonly admixed to a metal powder mixture in fractions of 0.5 to 2 wt.%, after which the blend is hot-consolidated and subsequently foamed by heating. As the alloy melts, TiH_2 decomposes, thereby releasing H_2 gas that creates bubbles [6]. The decomposition of TiH_2 is therefore important to understand. Precursors are heated up to temperatures sufficient to melt the alloy – 430 to 650 °C for the examples mentioned – and to initiate H_2 release. Isochronal decomposition of as-received TiH_2 powder takes place in various stages in which H_2 release peaks. The stages are correlated to phase transformations in TiH_2, start at about 370-380 °C and end at about 950 °C [7, 8, 9]. During foaming, however,

decomposition is mostly interrupted. The associated partial decomposition of TiH_2 has been studied ex-situ by X-ray diffraction [10] but not yet in-situ. Thus, understanding partial decomposition of TiH_2 is important to further improve metal foam manufacture.

For this study, we followed in-situ the phase transformations of TiH_2 powder and compared them to thermoanalytical traces obtained under equal temperature and atmospheric conditions. We quantified volume fractions of phases after partial decomposition and determined non-destructively their spatial distribution inside single particles with sub-µm resolution by using scanning X-ray tomography with powder diffraction-based contrast (XRD-µCT) [11, 12].

As-received TiH_2 powder (supplied by Chemetall GmbH, Frankfurt, particle size <36 µm) was both heated and cooled under flowing Ar. The phase transformations were followed in-situ by energy dispersive X-ray diffraction (ED-XRD) at the EDDI experimental station hosted at the synchrotron facility BESSY II of the Helmholtz Centre Berlin [13]. We illuminated the samples with a white beam of X-rays and the energy of diffracted photons was measured in transmission at a fixed $2\theta = 8°$ by a multi-channel analysing detector. Powder samples were poured into an alumina crucible of 5 mm diameter. We inserted a thermocouple through a hole in the crucible wall for measuring the sample temperature T_S. The crucible was tightened to the heating plate of an Anton Paar DHS 1100 furnace. A second thermocouple measured temperature of the heater T_H. A thin graphite dome closed the furnace chamber. After evacuation and backfill with Ar gas, a gas pressure of 1.2 bar at the inlet induced Ar flow through the chamber. The heater's temperature was increased from 30 to 680 °C at 10 $K \cdot min^{-1}$, then the heater was turned off and natural cooling took place. One spectrum was acquired every 12.4 s. Additional spectra were acquired for 60 s after cooling for quantitative phase analysis.

Simultaneous thermogravimetry and mass spectroscopy (TG-MS) were conducted in a Netzsch 209 C thermobalance coupled via a capillary to a quadrupole mass spectrometer QMS 209. We poured 90 mg of TiH_2 powder into an alumina crucible. Samples were heated at 10 $K \cdot min^{-1}$ from 35 to 620 °C and cooled at 40 $K \cdot min^{-1}$ under flowing Ar atmosphere. Differential scanning calorimetry (DSC) was done in a Netzsch STA 204 C applying identical temperature profile and atmosphere as for TG-MS.

The spatial distribution of phases inside individual particles was characterised non-destructively after ED-XRD by scanning X-ray microtomography at the nano-station ID22NI of the European Synchrotron Radiation Facility [14]. ID22NI was operated in monochromatic mode (17.5 keV photon energy). The X-rays were focused by multilayer-coated KB-optics to a spot size of 140 nm × 200 nm (h × v, FWHM). Tomographic scans were performed by scanning lines of the slice of interest horizontally (150 points, 260 nm step size), then rotated by 3°, and scanned again until a 180° rotation was completed. For each point of the scans, the powder diffraction pattern was collected. The software package XRDUA was employed for data processing [15]. Additionally, the sample was scanned using full-field microtomography at the ESRF beamline ID19 (0.3 μm pixel size, 17.6 keV).

Further microstructural characterisation was done by scanning electron microscopy (SEM) in a Zeiss SUPRA VP operated at 10 kV accelerating voltage. For this, the powders were mixed with an epoxy resin and cast. After curing, samples were ground and polished.

Fig.1 a shows the density map of diffraction intensities dispersed in energies as function of time obtained while heating and cooling the TiH_2 powder under flowing Ar. The profiles $T_H(t)$ and $T_S(t)$ depart from one another with increasing temperature because heat conduction through the powder sample decreases. Temperatures linked to diffraction lines correspond to $T_S(t)$. Temperatures of individual transformations are averaged values from different samples.

The starting phase δ belongs to the cubic space group (s.g.) $Fm\bar{3}m$, in which Ti atoms form a fcc sublattice and H atoms sit on tetrahedral sites [16]. As temperature increases the two hydrogen solid solutions α and β appear. α is hcp (s.g. $P6_3mmc$), β bcc (s.g. $Im\bar{3}m$) and in both, H atoms randomly occupy tetrahedral sites [16]. According to Fig. 1 a, the phase transformation sequence is:

$$\begin{cases} \text{heating}: \delta \xrightarrow{427\pm12\,^\circ\text{C}} \delta+\alpha \xrightarrow{508\pm14\,^\circ\text{C}} \delta+\alpha+\beta \xrightarrow{530\pm7\,^\circ\text{C}} \alpha+\beta \\ \text{cooling}: \alpha+\beta \xrightarrow{232\pm7\,^\circ\text{C}} \alpha+\delta \end{cases}$$

Sequential fittings for the diffraction lines δ_{220}, δ_{200}, α_{101}, α_{102} and β_{200} render $E_{i_{hkl}}$ values which via Bragg's law yield $d_{i_{hkl}}$ values and, from these, lattice parameters [17] whose time and temperature dependence is given in Fig. 1 b. Details of the

calculations are given in Supplement A. During heating, a_δ expands linearly up to 375 ± 5 °C. After this, a_δ contracts until δ vanishes. The lattice parameters a_β and c_α also decrease during heating, whereas a_α remains fairly constant. During cooling, both c_α and a_α contract continuously but a_β expands below 497 ± 15 °C. When a_β vanishes at 232 ± 7 °C, a_δ reappears and fluctuates around 4.405 Å.

The evolution of integrated intensities $I_{i_{hkl}}$ (i = α, β or δ) with time and temperature for the diffraction lines δ_{200}, α_{101} and β_{200}, is also presented in Fig. 1 b. They are proportional to the evolution of corresponding volume fractions f_{vi} of the phases [18].

Analysis of the ED diffraction spectrum after cooling yields volume fractions V_α = 68.9 % and V_δ = 31.1 % with standard deviations of 3.3 % using the intensities $I_{i_{hkl}}$ of the peaks marked by arrows in Fig. 1c, bottom and Supplement A [18]. This spectrum obtained at EDDI corresponds to a powder sample containing a large number of particles, whereas the diffractogram obtained at ID22NI (also given in Fig. 1 c) is the summed pattern of the whole XRD-μCT scanned section inside a cluster of just a few particles. Both patterns are in good agreement. Fig. 2 a1 depicts the size and morphology of the scanned particle cluster. Fig. 2 a2 represents the XRD-μCT reconstruction of the scanned section using the complete pattern given in Fig. 1 c, top. In this reconstruction the phases α and δ are not distinguishable, but the complex geometry of the particles and their variable sizes are visible. Fig. 2 a3 and a4 show individual spatial distributions of α and δ in the scanned section. Both phases are heterogeneously distributed and α occupies a larger area of the section than δ. Fig. 2 a5 is the combined map of both α and δ in which δ-rich regions appear surrounded by or adjacent to wider α-rich areas (see e.g. encircled region).

The microstructural analysis conducted by SEM is given in Fig. 2 b. The microstructure comprises a heterogeneous distribution of bright both coarse and thin lamellae, indicated as ***cL*** and ***tL*** respectively, embedded in a darker matrix ***M***. The inset contains an enlargement to show that ***tL*** are often parallel to each another, have clearer orientation and flatter boundaries with respect to the matrix than ***cL***.

TG-MS and DSC traces are summarized in Fig. 3. The mass = 2 ion current $I_{m=2}$ is an instantaneous measure of the H_2 gas release and is proportional to the mass change rate, i.e. $I_{m=2} \propto -\partial(\Delta m)/\partial t$ [7]. The H_2 gas release starts at 380 °C, has a multi-

peak structure during heating and decays fast when cooling starts. The mass change Δm reached -2.6 % during heating and remained fairly constant upon cooling. The heat flow trace resembles $I_{m=2}$ during heating as expected [7], but has a distinctive exothermic peak with onset at 230 °C during cooling.

As recently reported, during heating under Ar flow, every endothermic peak of H_2 release and the associated mass loss is correlated with contraction regimes of lattice parameters [9]. Dehydrogenation accompanied by mass loss starts when the lattice parameter a_δ starts to contract at 375 ± 5 °C (see a_δ in Fig. 1 b and onset temperature 380 °C in Fig. 3). We clarified in that work and confirm in the present one that the removal of H_2 gas by Ar flow favours the formation and persistence of an α-shell around a δ/β-core because α has the lowest H solubility S_H^α (see Fig. 4) and therefore, is the phase most compatible with the atmosphere [9]. In such a core-shell structure there is a hydrogen concentration C_H gradient within the particles – C_H is lower at the surface in the α shell than in the δ/β core. This is linked to the H solubility ranking for the three phases $S_H^\alpha < S_H^\beta < S_H^\delta$ as inferred from Fig. 4 [9]. This C_H gradient enables the co-existence of α+β+δ which otherwise would not be possible in the eutectoid Ti-H system given in Fig. 4 [7, 8, 9].

For complete dehydrogenation, α is the final phase and no transformation occurs during cooling [8, 9]. There is no phase transformation either if cooling starts from lower temperatures in which there is only α+δ, i.e. before β appears (Supplement B). In the present work, we start cooling from 616 ± 5 °C when β is the predominant phase (Fig. 1 b). From this condition the phase transformation $\alpha+\beta \xrightarrow{232\pm7\,^\circ\mathrm{C}} \alpha+\delta$ takes place because in the Ti-H system β cannot be retained by natural cooling or water quenching [10]. This transformation contains the eutectoid reaction β → α+δ which is shifted by –70 K with respect to the equilibrium temperature of 300°C due to continuous cooling at 40 K·min^{-1} [16] and is correlated with the exothermic peak shown in Fig. 3.

In principle, we could describe the cooling path by dropping an arrow from 616 °C for the remaining 1.2 wt.% H (3.8 (total) – 2.6 (mass loss) = 1.2) as done in Fig. 4. If the sample were in equilibrium at 616 °C, only β should be present, but in reality, when cooling starts α+β is found due to the stabilization of α by continuous

hydrogen removal through Ar flow [9]. This is one of the reasons why the resulting α:δ ratio is 75:25 (in wt.%, equivalent to 70:30 in vol.%) instead of the theoretical 60:40 inferred from the Ti-H phase diagram for C_H of 1.2 wt.% H indicated in Fig. 4.

Despite the fact that the cooling rate is 4 times higher than the heating rate at around 232 °C, mass conservation suppresses the C_H gradient and thus the co-existence of α+β+δ, as one would expect from the cooling path indicated in Fig. 4. The uncertainty for the transformation temperature 232 ± 7 °C originates from the scatter between measurements, but all individual measurements show no co-existence of α+β+δ during cooling as in Fig. 1a and b (see analogous to Fig. 1a but for another sample in Supplement C).

The cooling path in Fig. 4 helps understanding the evolution of volume fractions and lattice parameters of phases as temperature decreases for this slightly hypoeutectoid composition. Just before cooling started at 616 ± 5 °C, $f_{v\beta}$ reached its maximum and $f_{v\alpha}$ a local minimum (see Fig. 1b). With decreasing temperature, $f_{v\alpha}$ increases and $f_{v\beta}$ decreases, which indicates that the sample behaves as if it were in the α+β field. This effect is attributed to the 1.37 wt.% oxygen content in this commercial powder [9], which is known to enlarge the α+β field as indicated in Fig. 4 [19]. Inside the α+β field, β enriches in H because $f_{v\alpha}$ increases and $f_{v\beta}$ decreases, but C_H is constant and also, the hydrogen solubility in β increases up to the eutectoid composition whereas the solubility of α decreases below 600 °C [16]. Due to this H enrichment, a_β expands below 497 ± 15 °C whereas a_α and c_α shrink continuously due to temperature and solubility reduction. The sudden transformation $\alpha+\beta \xrightarrow{232\pm7\,^{\circ}C} \alpha+\delta$ involves also a quick and substantial increase of $f_{v\alpha}$ which subsequently reaches a maximum value. $f_{v\delta}$ remains fairly constant since it reappears as expected after entering the α+δ field.

A comparison between Fig. 2 a5 and Fig. 2 b, considering that the volumes are related as α:δ = 70:30, indicates that in the resulting microstructure the matrix is α and the lamellae are δ. In the core-shell model proposed in Ref. 9 for an average particle of 6 µm diameter, α would occupy a shell of about 0.2 µm thickness at 616 °C and cover a β core. TEM investigations showed that cooling down from 430 °C a

core-shell structure comprising an α shell surrounding a δ core can be retained, because no phase transformation occurs during cooling. But cooling down from 616 °C involves the eutectoid transformation of β in most of the particle volume, which prevents a high temperature core-shell structure to be retained. This leads to the resulting heterogeneous distribution of α and δ in which ***cL*** precipitate before ***tL*** and therefore, grow and loose interfacial coherence with respect to the matrix [20]. If such a core-shell distribution of phases after cooling existed, the non-destructive XRD-μCT analysis would certainly have detected it, as similar studies suggest [21], but no such observation was made.

In summary, during *heating*, endothermic peaks and their associated mass changes are correlated with individual phase transformations and regimes of lattice parameter contraction. Simultaneous temperature increase and H_2 removal by flowing Ar creates a hydrogen concentration gradient inside the particles and a core-shell structure of phases in which α+δ+β co-exist. When *cooling* starts at 616 ± 5 °C, there is no further mass loss and the phase transformation $\alpha+\beta \xrightarrow{232\pm7\,^{\circ}C} \alpha+\delta$ is correlated with an exothermic peak. Due to mass conservation and the large volume fraction β occupies before cooling starts, the co-existence of α+δ+β is suppressed. No evidence of an existing α-shell/β-core at high temperatures remains and the resulting microstructure is a heterogeneous distribution of δ-lamellae embedded in an α-matrix in volume proportions α:δ = 70:30.

We thank H. Kropf for providing the SEM images.

References

[1] F. Garcia-Moreno, M. Fromme, J. Banhart, Adv. Eng. Mater. 2004, 6, 416.

[2] F. Garcia-Moreno, C. Jiménez, M. Mukherjee, P. Holm, J. Weise, J. Banhart, Colloids and Surfaces A, 2009, 344, 101.

[3] K. Kitazono, Y. Takiguchi, Scripta Mater. 2006, 55, 501.

[4] A. Chethan, F. Garcia-Moreno, N. Wanderka, B.S. Murty, J. Banhart, J Mater Sci 2011, 46, 7806.

[5] W. Bach, D. Bormann, P. Wilk, R. Kucharski, Cellular Matals and Polymers, Eds.: R.F. Singer, C. Körner, V. Altstädt, H. Münstedt, Trans Tech Publications, Zürich, 2005, 77.

[6] J. Baumeister, German Patent DE40 18 360, 1990.

[7] B. Matijasevic-Lux, J. Banhart, S. Fiechter, O. Görke, N. Wanderka, Acta Mater 2006; 54: 1887.

[8] H. Liu, P. He, J.C. Feng, J Cao. Int J Hydrogen Energy 2010; 34: 3018.

[9] C. Jiménez, F. Garcia-Moreno, B. Pfretzschner, M. Klaus, M. Wollgarten, I. Zizak, G. Schumacher, M. Tovar, J. Banhart, Acta Mater 2011, 56, 6318.

[10] Ch. Borchers, T.I. Khomenko, A.V. Leonov, O.S. Morozova, Thermochim Acta 2009, 493, 80.

[11] P. Bleuet, E. Welcomme, E. Dooryhée, J. Susini, J.-L. Hodeau, Ph. Walter, Nature Mater 2008, 7, 468.

[12] S.R. Stock, F. De Carlo, J.D. Almer, J Struct. Biol. 2008, 161, 144.

[13] Ch. Genzel, I. Denks, J. Gibmeier, M. Klaus, G. Wagener, Nucl Instr and Meth in Phys Res A 2007, 578, 23.

[14] G. Martinez-Criado, R. Tucoulou, P. Cloetens, P. Bleuet, J Sychrotron Radiat 2011, submitted.

[15] W. De Nolf and K. Janssens, Surf. Interface Anal., 2010, 42, 411.

[16] A. San Martin, F.D. Manchester. Bull Alloy Phase Diag 1987; 8: 30.

[17] B.D. Cullity. Elements of X-Ray Diffraction. Reading: Addison-Wesley; 1978.

[18] E.S.U. Laine, J Phys F: Metal Phys, 1978, 8, 1343.

[19] W.M. Müller. Titanium Hydrides, in: W.M. Müller, Blackledge JP, G.G. Libowitz (Eds.). Metal Hydrides. New York: Academic Press; 1968.

[20] K.E. Easterling, Phase Transformations in Metals and Alloys. London: Chapman and Hall; 1981

[21] C. Mochales, A. Maerten, A. Rack, P. Cloetens, W.D. Mueller, P. Zaslansky, C. Fleck, Acta Biomater. 2011, 7, 2994.

Fig. 1a – Density map of diffracted intensities dispersed in energies given as function of time. The evolution of the phases δ, β and α during heating and cooling under Ar flow is shown. Number triples are hkl indices. Temperatures derive from $T_S(t)$. b –

Evolution of lattice parameters and integrated intensities and $T_S(t)$. c – Diffractograms obtained after cooling using the instruments EDDI and ID22NI.

Fig. 2 – Top: a1 – Microtomogram of the scanned particle cluster. a2 – XRD-µCT reconstruction based on the entire diffraction pattern given in Fig. 1 c. Bottom: spatial distributions of δ (a3) and α (a4) phases as well as the combination of both (a5). b – Microstructure of particles after cooling as seen by SEM.

Fig. 3 – Thermoanalytical DSC combined with gravimetric/mass-spectroscopic traces (Δm and $I_{m=2}$) of TiH_2 powders heated up to 620 °C and cooled down under Ar flow. Top: measured temperatures profiles $T_{TG\text{-}MS}(t)$ and $T_{DSC}(t)$.

Fig. 4 – Phase diagram of the Ti-H system [16]. Lines extending the α+β field within 600-900 °C and 0-30 at.% H are taken from Ref. 19. Remaining H at 616 °C is 1.2 wt.%. The red arrow indicates the equilibrium cooling path.

Fig1

Click here to download high resolution image

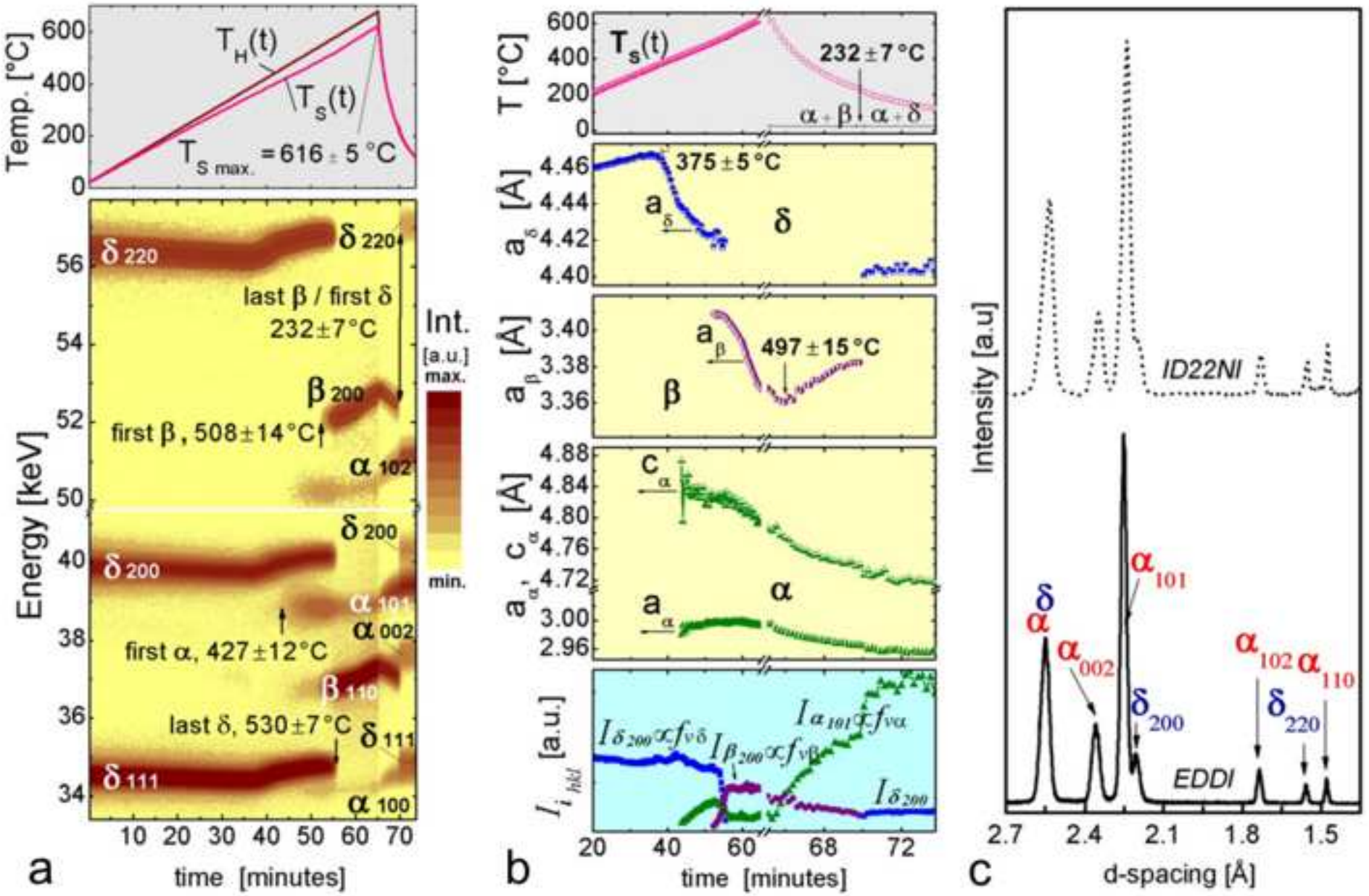

Fig2

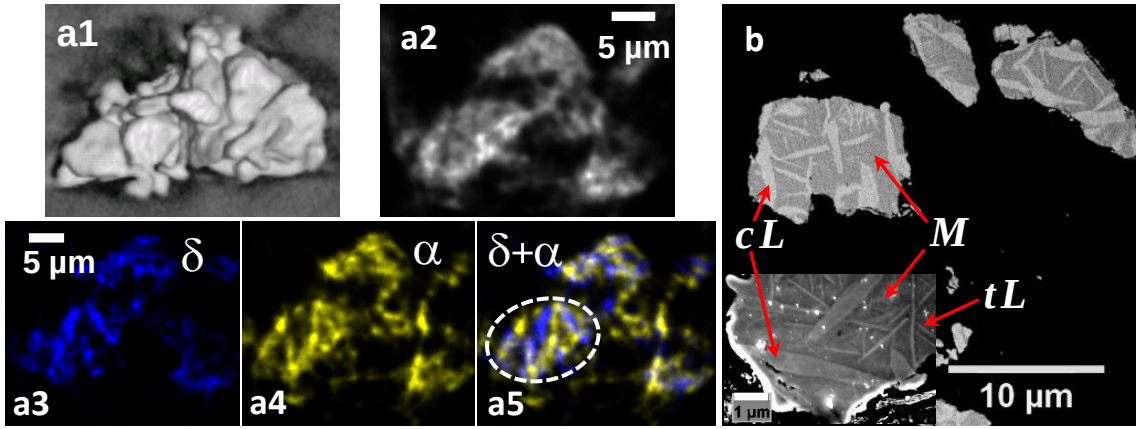

Fig3

Click here to download high resolution image

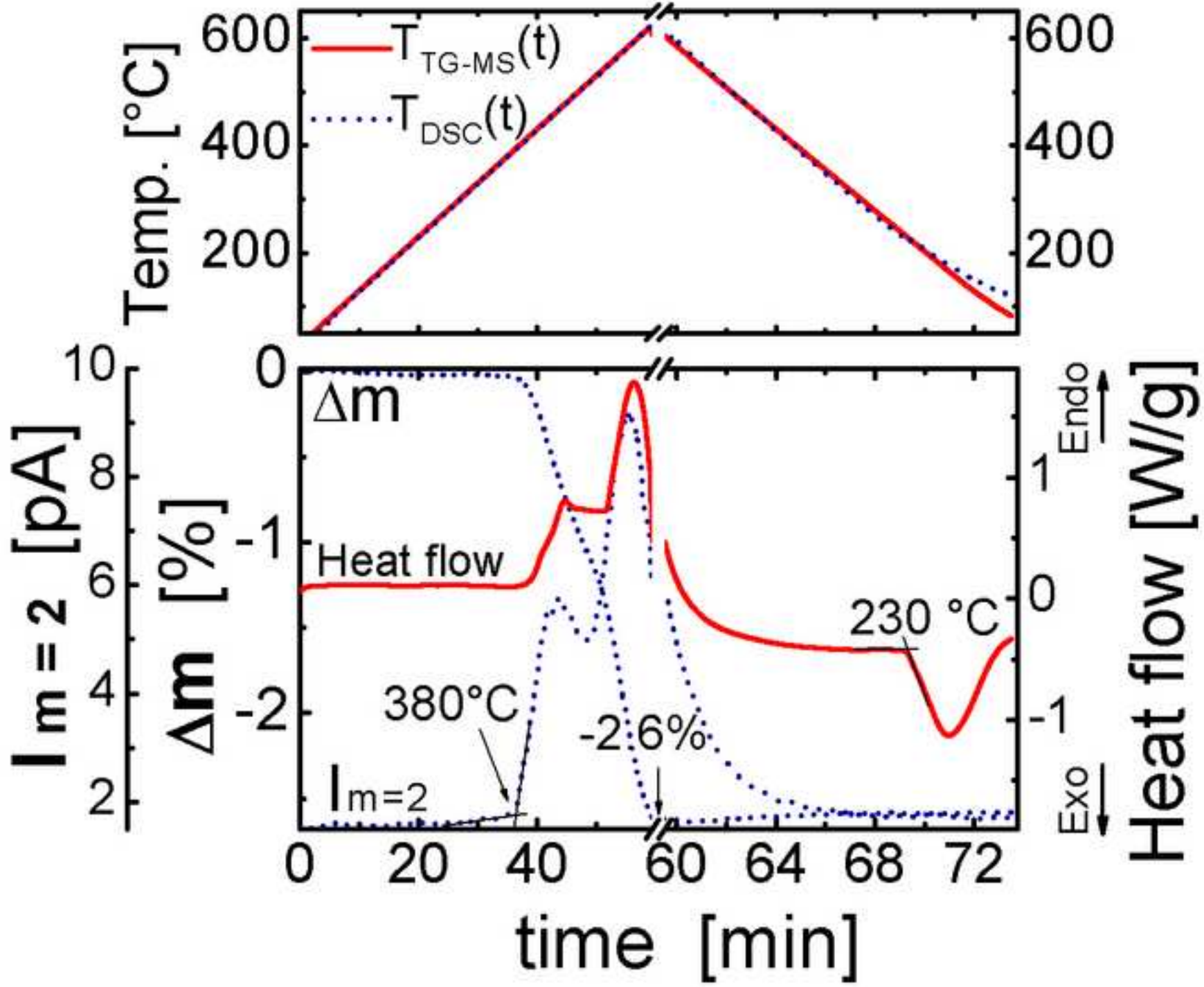

Fig4

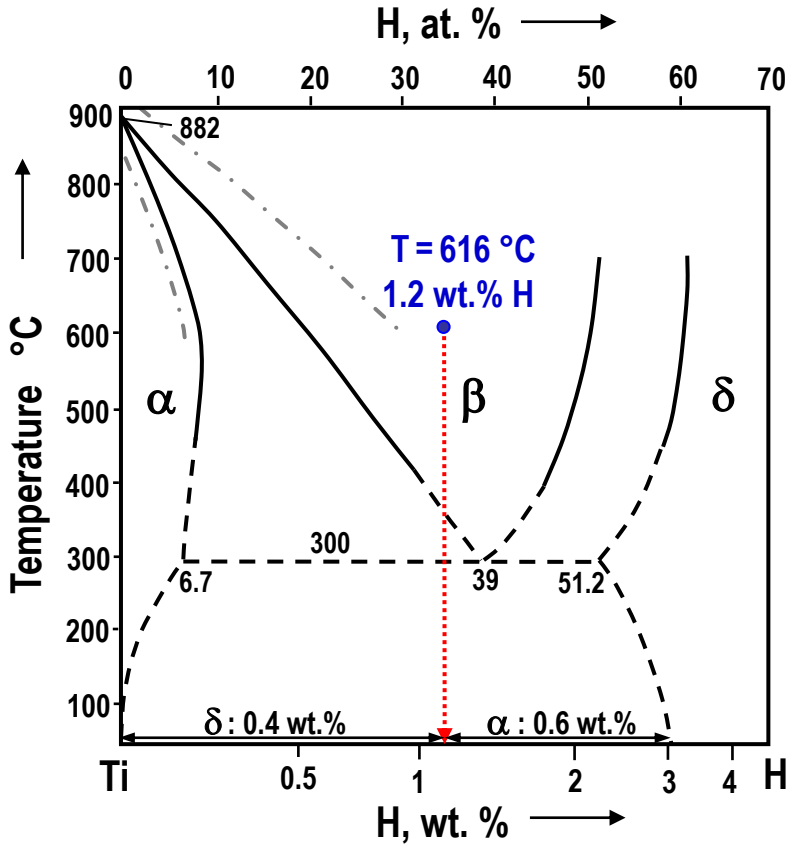
H, at. %
0
10
20
30
40
50
60
70
900
800
700
600
500
400
300
200
100
882
T = 616 °C
1.2 wt.% H
α
β
δ
Temperature °C
300
6.7
39
51.2
δ : 0.4 wt.%
α : 0.6 wt.%
Ti
0.5
1
2
3
4
H
H, wt. %

SupplementA

Click here to download Supplementary Material: Supplement_A.doc

SupplementB

Click here to download Supplementary Material: Supplement_B.jpg

SupplementC

Click here to download Supplementary Material: Supplement_C.jpg